Atmos. Chem. Phys. Discuss., doi:10.5194/acp-2017-295, 2017
Manuscript under review for journal Atmos. Chem. Phys.
Discussion started: 29 May 2017

Atmospheric Chemistry and Physics
Discussions

Mixing layer height on the North China Plain and meteorological evidence of serious air pollution in southern Hebei

Xiaowan Zhu[1,3], Guiqian Tang[1,2*], Jianping Guo[4], Bo Hu[1], Tao Song[1], Lili Wang[1], Jinyuan Xin[1], Wenkang Gao[1], Christoph Münkel[5], Klaus Schäfer[6], Xin Li[1,7], and Yuesi Wang[1]

[1]State Key Laboratory of Atmospheric Boundary Layer Physics and Atmospheric Chemistry (LAPC), Institute of Atmospheric Physics, Chinese Academy of Sciences, Beijing 100029, China
[2]Center for Excellence in Regional Atmospheric Environment, Institute of Urban Environment, Chinese Academy of Sciences, Xiamen 361021, China
[3]University of Chinese Academy of Sciences, Beijing 10049, China
[4]State Key Laboratory of Severe Weather & Key Laboratory of Atmospheric Chemistry of CMA, Chinese Academy of Meteorological Sciences, Beijing 100081, China
[5]Vaisala GmbH, 22607 Hamburg, Germany
[6]Atmospheric Science College, Chengdu University of Information Technology (CUIT), Chengdu 610225, China
[7]Beijing Municipal Committee of China Association for Promoting Democracy, Beijing 100035, China

Correspondence to: G. Tang (tgq@dq.cern.ac.cn)

Abstract

To investigate the spatiotemporal variability of regional mixing layer height (MLH) on the North China Plain (NCP), multi-site and long-term observations of MLH with ceilometers at three inland stations [e.g., Beijing (BJ), Shijiazhuang (SJZ), Tianjin (TJ)] and one coastal site [e.g., Qinhuangdao (QHD)] were conducted from 16 October 2013 to 15 July 2015. The MLH at the inland stations on the NCP were highest in summer and lowest in winter, while the MLH in the coastal area of Bohai was lowest in summer and highest in spring. The regional MLH developed the earliest in summer (at approximately 7:00 LT) and reached the highest growth rates (164.5 m h^{-1}) at approximately 11:00 LT, while in winter, the regional MLH developed much later (at approximately 9:00 LT), with the maximum growth rates (101.8 m h^{-1}) occurring at 11:00 LT. As a typical site in southern Hebei, the annual mean of MLH at SJZ was 464±183 m, which was 15.0 % and 21.9 % lower than that at the BJ (594±183 m) and TJ (546±197 m) stations, respectively. Investigation of radiation and wind shear at NCP revealed that the net radiation was almost consistent on a regional scale, and the lower MLH in southern Hebei was mainly due to the 1.9-2.8-fold higher intensity of wind shear on the northern NCP than in southern Hebei at an altitude of 300-1700 m. Furthermore, the ventilation coefficient and the relative humidity in southern Hebei were 1.1-2.1 times smaller and 13.2-22.1 % higher than

that on the northern NCP, respectively. As a result, severe haze pollution occurred much more readily in southern Hebei and the annual means of near-ground $PM_{2.5}$ concentrations were almost 1.3 times higher than those of the northern areas. Due to the unfavorable weather conditions, industrial capacity should be reduced in southern Hebei, heavily polluting enterprises should be relocated and strong emission reduction measures are required to improve the air quality.

1. Introduction

The convective boundary layer is the region where turbulence is fully developed. The height of the interface where turbulence is discontinuous is usually referred to as the mixing layer height (MLH) (Stull, 1988). The mixing layer is regarded as the link between the near-surface and free atmosphere, and the MLH is one of the major factors affecting atmospheric dissipation ability, which determines both the volume into which ground-emitted pollutants can disperse, as well as the convective time scales within the mixing layer (Seidel et al., 2010). In addition, continuous MLH observations will be of great importance for the improvement of boundary layer parameterization schemes and for the promotion of meteorological model accuracy.

Conventionally, the MLH is usually estimated from radiosonde profiles (Seidel et al., 2010). Although meteorological radiosonde observations can provide high-quality data, they are not suitable for continuous fine-resolution MLH retrievals due to their high cost and limited observation intervals (Seibert et al., 2000). As the most advanced method of MLH detection, remote sensing techniques based on the profile measurements from ground-based instruments such as sodar, radar, or lidar that have the unique vertically resolved observational capability are becoming increasingly popular (Beyrich, 1997; Chen et al., 2001; He et al., 2005). Because sound waves can be easily attenuated in the atmosphere, the vertical range of sodar is generally limited to within 1000 m. However, the optical remote sensing techniques can provide higher height ranges (at least several kilometers). The single-lens ceilometers developed by Vaisala have been widely used in a variety of MLH studies (e.g., Emeis et al., 2004; Emeis et al., 2009; Emeis et al., 2011; Eresmaa et al., 2006; Münkel et al., 2006; Muñoz and Undurraga, 2010; Munkel and Rasanen, 2004; Schween et al., 2014; Sokół et al., 2014; Tang et al., 2016; Tang et al., 2015b). Compared with other remote sensing instruments, this type of lidar has special features favorable for long-term and multi-station observations (Emeis et al., 2009; Wiegner et al., 2014; Tang et al., 2016), including the low-power system, the eye-safe operation within a near infrared laser band, and the low cost and ease of maintenance during any weather conditions (excluding rainy, strong windy or sandstorm weather conditions) with only regular window cleaning required (Emeis et al., 2004; Tang et al., 2016).

The North China Plain (NCP) region is the political, economic and cultural center of China. With the rapid economic development, energy use has increased substantially, resulting in frequent air pollution episodes (e.g., Guo et al., 2011; Li et al., 2013; Liu et al., 2016; Tang et al., 2015a; Wang et al., 2014; Wang et al., 2013; Xu et al., 2016; Zhang et al., 2014). The haze pollution has had an adverse impact on human health (Tang et al., 2017a) and has aroused a great deal of concern (Tang et al., 2009; Ji et al., 2012; Zhang et al., 2015). To achieve the integrated of development of the Jing-Jin-Ji region, readjustment of the regional industrial structure and layout is imperative. To this end, the industrial capacity of heavily polluting enterprises in the areas with unfavorable weather conditions should be reduced, and these heavily polluting enterprises should be removed to improve the air quality. For the remaining enterprises, the industrial air pollutant emissions structure should be changed, and strong emission reduction measures must be implemented. Although the government has carried out some strategies for joint prevention and control, with the less well-understood distributions of regional weather condition status on the NCP, how and where to adjust the industrial structures on the NCP are questions in pressing need of answers. As one of the key factors influencing the regional heavy haze pollution (Tang et al., 2012; Quan et al., 2013; Hu et al., 2014; Tang et al., 2016; Zhu et al., 2016; Tang et al., 2017b; Zhang et al., 2016), the MLH to some extent represents the atmospheric environment capacity, and the regional distribution and variation of MLH in the NCP can offer a scientific basis for regional industrial distribution readjustment, which will be of great importance for regional haze management.

Nevertheless, due to the scarcity of MLH observations on the NCP, reliable and explicit characteristics of MLH on the NCP remain unknown. Tang et al. (2016) utilized the long-term observation data of MLH from ceilometers to analyze the characteristics of MLH variations in Beijing (BJ) and verified the reliability of ceilometers. The results demonstrated that MLH in BJ was high in spring and summer and low in autumn and winter with two transition months in February and September. A multi-station analysis of MLH in the NCP region was conducted in February 2014, and the characteristics of high MLH at coastal stations and low MLH at southwest piedmont stations were reported (Li et al., 2015). Miao et al. (2015) modeled the seasonal variations of MLH on the NCP and discovered that the MLH was high in spring due to the strong mechanical forcing and low in winter as a result of the strong thermodynamic stability in the near-surface layer. The mountain-plain breeze and the sea breeze circulations played an important role in the mixing layer process when the background synoptic patterns were weak in summer and autumn (Tang et al., 2016).

However, the regional MLH simulation analysis is incomplete without verification with long-term measured MLH data. To overcome previous studies' deficiencies, our study first conducted a 22-months (from 16 October 2013 to 15 July 2015) observation of MLH with ceilometers on the NCP. The observation stations included three inland stations [e.g., BJ, Shijiazhuang (SJZ) and Tianjin (TJ)] and one coastal site [e.g., Qinhuangdao (QHD)]. First, we will describe the spatial and temporal distribution of MLH on the NCP. Subsequently, reasons for MLH differences on the NCP will be explained in the discussion section. Finally, the weather conditions on the NCP are described to provide a scientific basis for regional industrial structure readjustment.

2 Data and methods

2.1 Sites

To study the regional MLH characteristics in the NCP region, observations with ceilometers were conducted at the BJ, SJZ, TJ and QHD stations (Fig. 1 and Table 1). The SJZ, TJ and QHD sites were set around Beijing in the east, southeast and southwest direction, respectively. The BJ station was at the base of the Taihang and Yanshan Mountains on the northern NCP. The MLH observation site was built in the courtyard of the Institute of Atmospheric Physics, Chinese Academy of Sciences (116.32° E, 39.90° N). SJZ was near the Taihang Mountain in southern Hebei; the location was in the Hebei University of Economics (114.26° E, 38.03° N). The TJ site was set in the courtyard of the Tianjin Meteorological Bureau, which was located south of the urban area, with a geographic location of 117.20° E, 39.13° N. The QHD station was an eastern coastal site of Bohai Bay, which was set up in the Environmental Management College of China (119.57° E, 39.95° N) and the surrounding areas are mostly residential buildings with no high structures.

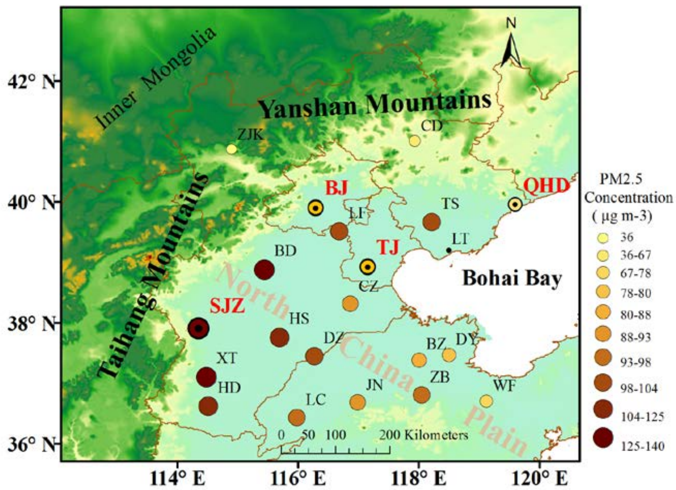

Fig. 1. Locations of the ceilometers observation sites (BJ, SJZ, TJ and QHD) are marked with red and bold abbreviations; other $PM_{2.5}$ observation sites (ZJK, CD, LF, TS, CZ, BD, HS, XT, HD, DZ, LC, JN, BZ, DY, ZB and WF) and the sounding observation sites (BJ, LT and XT) are marked on the map with black abbreviations. The size and color of the circular mark are representatives of the annual mean of near-ground $PM_{2.5}$ concentration; the larger and darker the circle, the greater the concentrations.

Atmos. Chem. Phys. Discuss., doi:10.5194/acp-2017-295, 2017
Manuscript under review for journal Atmos. Chem. Phys.
Discussion started: 29 May 2017

Table 1. Specific information of the observation sites on the NCP.

Cityname	Abbreviation	Province or municipality	Longitude	Latitude
Beijing[a,b,c]	BJ	Beijing	116.32° E	39.90° N
Tianjin[a,b]	TJ	Tianjin	117.20° E	39.13° N
Shijiazhuang[a,b]	SJZ	Hebei	114.26° E	38.03° N
Langfang[a]	LF	Hebei	116.70° E	39.53° N
Tangshan[a]	TS	Hebei	118.02° E	39.68° N
Qinhuangdao[a,b]	QHD	Hebei	119.57° E	39.95° N
Zhangjiakou[a]	ZJK	Hebei	114.92° E	40.90° N
Chengde[a]	CD	Hebei	117.89° E	40.97° N
Laoting[b,c]	LT	Hebei	118.90° E	39.31° N
Cangzhou[a]	CZ	Hebei	116.83° E	38.33° N
Baoding[a]	BD	Hebei	115.48° E	38.85° N
Hengshui[a]	HS	Hebei	115.72° E	37.72° N
Xingtai[b,c]	XT	Hebei	114.48° E	37.05° N
Handan[a]	HD	Hebei	114.47° E	36.60° N
Dezhou[a]	DZ	Shandong	116.29° E	37.45° N
Liaocheng[a]	LC	Shandong	115.97° E	36.45° N
Jinan[a]	JN	Shandong	116.98° E	36.67° N
Binzhou[a]	BZ	Shandong	118.02° E	37.22° N
Dongying[a]	DY	Shandong	118.49° E	37.46° N
Zibo[a]	ZB	Shandong	118.05° E	36.78° N
Weifang[a]	WF	Shandong	119.06° E	36.68° N

[a]Ceilometer observation sites.
[b]Near-ground $PM_{2.5}$ concentration sites.
[c]Radiosonde observation sites.

2.2 Measurement of MLH

The instrument used to measure the MLH at the four stations was an enhanced single-lens ceilometer (Vaisala, Finland), which utilized the strobe laser lidar (laser detection and range measurement) technique (910 nm) to measure the attenuated backscattering coefficient profiles. As large differences existed in the aerosol concentrations between the mixing layer and the free atmosphere, the MLH can be determined from the vertical attenuated backscattering coefficient (β) gradient, whereby a strong, sudden change in the negative gradient (-dβ/dx) can indicate the MLH. In the present study, the Vaisala software product BL-VIEW was utilized to calculate the MLH by determining the location of the maximum -dβ/dx in the attenuated backscattering coefficient. To strengthen the echo signals and reduce the detection noise, spatial and temporal averaging should be conducted before the gradient method is used to calculate the MLH. The BL-VIEW software was utilized with temporal smoothing of 1200 s and vertical distance smoothing of 240 m. The instrument installed at the BJ station was a CL31 ceilometer and the CL51 ceilometers were used at the SJZ, TJ and QHD stations. Some of the properties of these two instruments are listed in Table 2, and basic technical descriptions can be found in Münkel et al. (2007) and Tang et al. (2015).

To ensure the consistency of the MLH measured with the two different versions of ceilometers, before we set up the ceilometers at different stations, we made a comparison of the MLH observed by CL31and CL51 at BJ from October 1 to October 8, 2013 (Fig. S1). The MLH observed by CL 31 was highly correlated with those observed by each of the three CL51 ceilometers, with relative correlation coefficients (R) of 0.92, 0.86 and 0.92. Therefore, the impact of version discrepancy on MLH measurement can be neglected.

Table 2. Instrument properties of CL31 and CL51

Parameter	CL31	CL51
Detection range (km)	7.7	13.0
Wavelength (nm)	910	910
Report period (s)	2-120	6-120
Report accuracy	5m	10m
Peak power (W)	310	310

2.3 Other data

The hourly data of relative humidity (RH), temperature (T), near-ground wind speed (WS) and direction at the BJ, SJZ, TJ and QHD stations were obtained from China Meteorological Administration (http://www.weather.com.cn/weather/101010100.shtml). Hourly net (0.2-100 μ m) radiation data at the BJ, TJ and SJZ sites were observed using a net radiometer (NR Lite2, Kipp & Zonen, Netherlands), detailed information is included in Hu et al., (2012). Because the SJZ and QHD stations are missing radio sounding data, sounding data from the XT and LT stations were used instead. Sounding data of WS and direction at the BJ, XT and LT stations were provided by the upgraded radiosonde network of China, where the GTS1 digital electronic radiosonde was required to be operationally launched twice per day at 08:00 LT and 20:00 LT by the China Meteorological Administration (Guo et al., 2016).

The near-ground $PM_{2.5}$ and PM_{10} concentrations at the 20 observation sites from December 2013 to November 2014 were provided by the Ministry of Environmental Protection (http://www.zhb.gov.cn/) with a time resolution of 1 h. Details for the near-ground $PM_{2.5}$ and PM_{10} observation sites are listed in Table 1 and Fig. 1.

3 Results

3.1 Frequency distribution of regional MLH

Continuous operation of the ceilometers since October 2013 has provided 22 months of data, and for the purpose of analyzing of the MLH variability in the NCP region, the hourly averages of MLH for a whole year (from December 2013 to November 2014) at the BJ, SJZ, TJ and QHD stations were utilized in the following study. Hourly means of MLH under rainy, sandstorm and windy conditions were removed (Muñoz and Undurraga, 2010; Tang et al., 2016; van der Kamp and McKendry, 2010), resulting in data availability of 81, 89, 83 and 77 % at the BJ, SJZ, TJ and QHD stations, respectively. The frequency distribution of daily maximum

Atmos. Chem. Phys. Discuss., doi:10.5194/acp-2017-295, 2017
Manuscript under review for journal Atmos. Chem. Phys.
Discussion started: 29 May 2017

Atmospheric Chemistry and Physics
Open Access
EGU
Discussions

MLH is shown in Fig. 2. In this study, March, April and May are defined as spring; June, July and August are defined as summer; September, October and November are defined as autumn; and December, January and February are defined as winter.

The daily maximum MLH at the BJ, SJZ and TJ stations reached 2400 m, and the high daily maximum values mostly occurred in spring and summer, while the low values occurred in autumn and winter and were as low as 200 m. The maximum MLH values at the BJ, SJZ and TJ stations were mainly distributed between 600 and 1800 m, 400 and 1600 m and 800 and 1800 m, respectively, and they accounted for 74.2, 72.0 and 67.0 % of the total samples, respectively. Notably, the daily maximum MLH at SJZ was lower in spring, autumn and winter in comparison with those at the BJ and TJ stations. Values below 600 m at the SJZ station occurred primarily in autumn and winter; the most frequent daily maximum MLH was in the range from 1000 to 1200 m, which was 200-600 m lower than that at the TJ station. This pattern demonstrated a weaker atmospheric diffusion capability at SJZ in spring, autumn and winter than at the northern stations.

The frequency distribution of the daily maximum MLH at the coastal station was different. The daily maximum MLH at QHD was mainly distributed between 800 and 1800 m with relatively uniform seasonal distributions (Fig. 2d). Values lower than 600 m mainly occurred in summer, which was probably influenced by the frequent occurrence of a thermal internal boundary layer in summer (van der Kamp and McKendry, 2010).

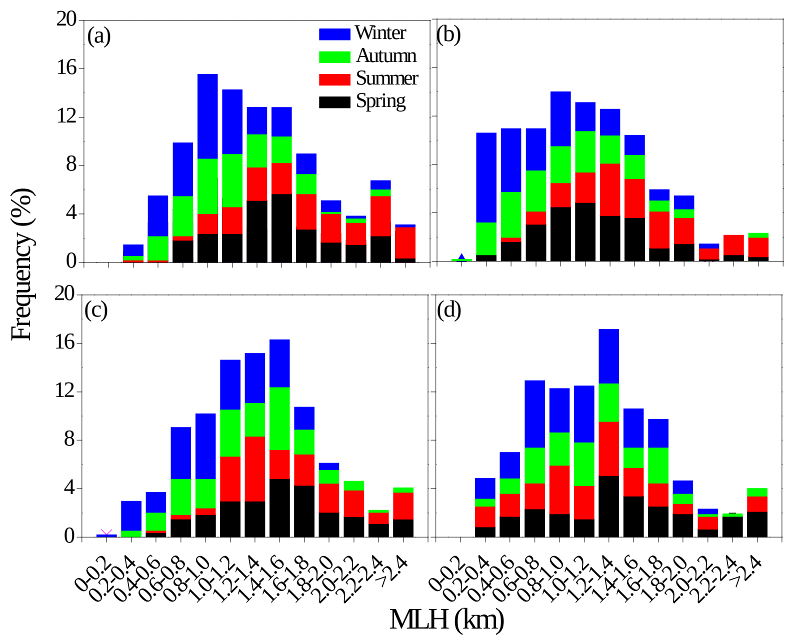

Fig. 2. Frequency distribution of daily maximum MLH at the (a) BJ, (b) SJZ, (c) TJ and (d) QHD stations from December 2013 to November 2014.

3.2 Spatiotemporal variation of regional MLH

3.2.1 Seasonal variation

Atmos. Chem. Phys. Discuss., doi:10.5194/acp-2017-295, 2017
Manuscript under review for journal Atmos. Chem. Phys.
Discussion started: 29 May 2017

Atmospheric Chemistry and Physics
Open Access
Discussions

Monthly variations of MLH at the BJ, SJZ, TJ and QHD stations are shown in Fig. 3. The monthly means of the regional MLH ranged between 300 and 750 m; the maximum and minimum MLH occurred in June 2014 at the BJ station and in January 2014 at the SJZ station, with values of 741 and 308 m, respectively. Most of the monthly averages were between 400 and 700 m, which accounted for 81.3 % of the total samples.

The MLH at the BJ, SJZ and TJ stations showed obvious seasonal variations with high values in spring and summer and low values in autumn and winter. Seasonal means of MLH at the three stations followed the same order: summer>spring>autumn>winter, with maximum values of 722±169, 623 ±161 and 655±165 m in summer, respectively, and minimum values of 493±131, 347±153 and 436±178 m in winter, respectively (Table S1). Obvious annual changes of the MLH with large amplitude at the BJ, SJZ and TJ stations implied that MLH is influenced by seasonal changes of solar radiation, and in summer, the intense solar radiation favors the development of MLH (Stull, 1988).

Nevertheless, the seasonal variation of MLH at the coastal site of Bohai was different from that at the inland stations. The MLH at QHD exhibited a decreasing trend from spring to summer and increasing trend from autumn to winter, and the maximum seasonal mean at QHD was 498±217 m in spring and the minimum was 447±153 m in summer. Moreover, the MLH in spring and summer at QHD was much lower than at other stations. Similar to our analysis of frequency distributions of daily maximum MLH in Section 3.1, the lower MLH at QHD in spring and summer mainly resulted from the frequent occurrence of sea breeze (Fig. 5). Under the influence of the abrupt change of aerodynamic roughness and temperature between the land and sea surfaces, a thermal internal boundary layer will occur frequently in the coastal areas, which will decrease the average MLH to some extent. This impact of sea breeze on the coastal boundary layer was consistent with previous studies (Zhang et al., 2013; Tu et al., 2012), which demonstrated that ceilometers can properly retrieve the coastal MLH as well.

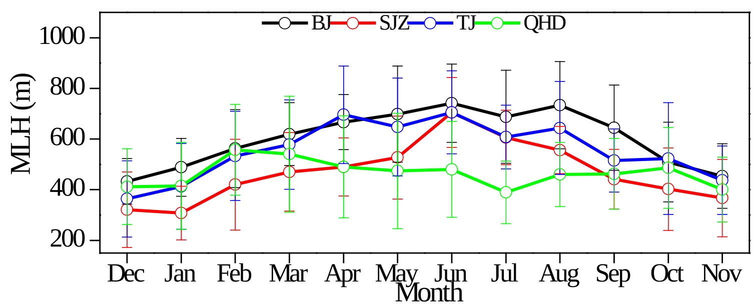

Fig. 3 Monthly variations of MLH at the BJ, SJZ, TJ and QHD stations from December 2013 to November 2014.

Annual averages of MLH at the BJ, SJZ, TJ and QHD stations were also calculated, and the values were 594±183, 464±183, 546±197 and 465±175 m, respectively. The MLH at SJZ was approximately 21.9, 15.0 and 0.2 % lower than at the BJ, TJ and

Atmos. Chem. Phys. Discuss., doi:10.5194/acp-2017-295, 2017
Manuscript under review for journal Atmos. Chem. Phys.
Discussion started: 29 May 2017

QHD stations, respectively, which revealed a more stable atmospheric stratification and weaker atmospheric environment capability in southern Hebei.

3.2.2 Diurnal variations

Seasonal variations of diurnal MLH change patterns were investigated to reveal the 24 h evolution characteristics of the regional MLH on the NCP. As shown in Fig. 4, diurnal variations of regional MLH in different seasons all had single peak patterns. With sunrise and increased solar radiation, MLH at the four stations started to develop and peaked in the early afternoon. After sunset, turbulence in the MLH decayed quickly, and the mixing layer underwent a transition to the nocturnal stable layer (less than 400 m). The averaged annual daily ranges of MLH at the BJ, SJZ, TJ and QHD stations were 782, 699, 914 and 790 m, respectively, and the averaged annual daily range of MLH at SJZ was 100-200 m smaller than at other stations. When we referred to the diurnal variations of regional MLH in different seasons, we found that the lower annual daily range at the SJZ station was associated with its lower values of daytime MLH in spring, autumn and winter (Figs. 4a, 4c and 4d).

Average growth rates for the four stations demonstrated that the growth rates of the regional MLH varied by season. The MLH developed earliest in summer (at approximately 7:00 LT) and reached the highest growth rates (164.5 m h^{-1}) at approximately 11:00 LT, and the time when MLH started to develop was found to be 1 hour later (at approximately 8:00 LT) in spring and autumn than in summer. Furthermore, the MLH developed the latest (at approximately 9:00 LT) and slowest in winter, with the maximum growth rate (101.8 m h^{-1}) occurring at approximately 11:00 LT.

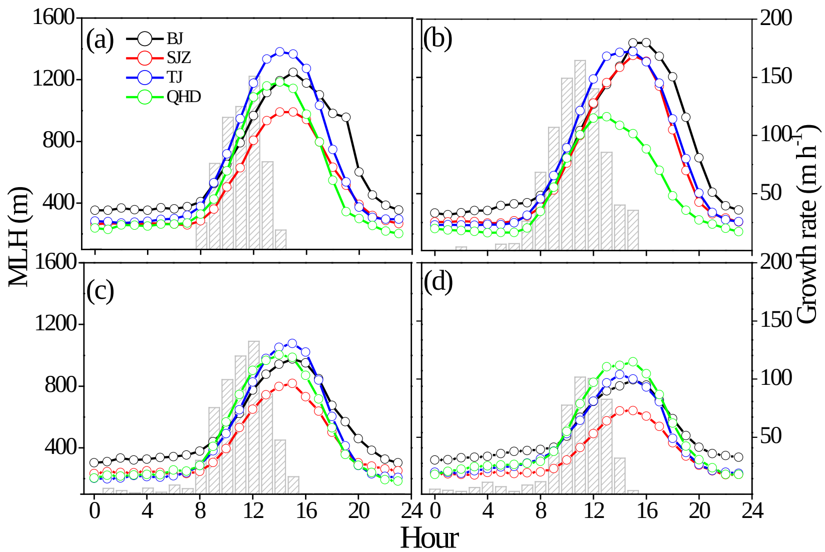

Fig. 4. Diurnal variations of MLH at the BJ, SJZ, TJ and QHD stations in (a) spring, (b) summer, (c) autumn and (d) winter seasons are indicated by lines and scatters. The averaged growth rates at the four sites are depicted with gray columns for each season to represent the regional MLH growth velocity, and only positive values are shown in

Atmos. Chem. Phys. Discuss., doi:10.5194/acp-2017-295, 2017
Manuscript under review for journal Atmos. Chem. Phys.
Discussion started: 29 May 2017

the figure.

Comparison of the MLH peaking time between the four stations showed that the maximum MLH at the TJ and QHD stations arrived earlier than at the BJ and SJZ stations in spring and summer (Figs. 4a and 4b). However, in autumn and winter, such a characteristic was not evident (Figs.4c and 4d).

As shown in Fig. 5, under the influence of the Siberian High and the geographic location effect, northerly and northwesterly winds prevailed in autumn and winter at the four stations. In spring and summer, the northward lift and westward intrusion of a subtropical high causes the weak southerly wind to arrive and dominate in the NCP region. Without a large- or medium-scale weather system passing through, the sea breeze will play a role in the coastal area. Although the TJ station was supposed to be an inland site, it was still affected by the sea breeze to some extent. Due to the shoreline orientation and regional topography differences between TJ and QHD (Fig. 1), when a sea breeze occurred, easterly wind prevailed at the former station and easterly, and south-southwesterly wind blew at the latter station in spring and summer (Figs.5c and 5d). Statistical results revealed that from March 2014 to August 2014, the frequency of sea breeze occurrence at the TJ and QHD stations could reach 53.8 and 92.4 %, respectively, and the sea breeze usually started at midday (approximately 11:00 LT).

Generally, the vertical development of the mixing layer is heavily reliant on the vertical turbulence, but when sea breeze is present, cool air advection from the sea breeze circulation will suppress this vertical mixing intensity (Puygrenier et al., 2005). The co-existence of vertical turbulence and advection caused the MLH to decrease and peak earlier. Meanwhile, the local mixing layer will be replaced by the thermal internal boundary layer (Tomasi et al., 2011). As a result, the earlier peaking time of MLH in spring and summer could be attributed to the sea breeze effect. The MLH peaking time at the TJ station was approximately 1-2 hours later than at the QHD station, which indicated that such a sea breeze impact will weaken with distance from the coast (Huang et al., 2016).

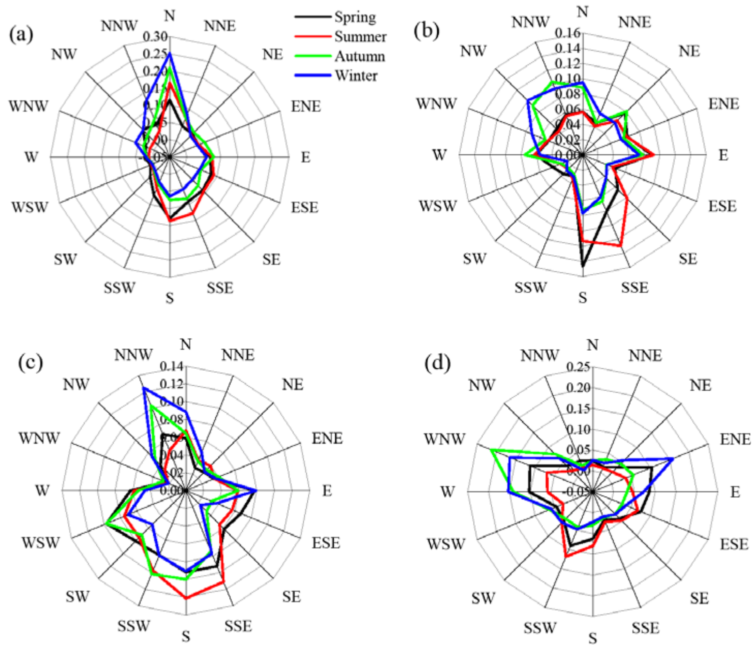

Fig. 5 Frequency of wind direction at the (a) BJ, (b) SJZ, (c) TJ and (d) QHD stations in different seasons.

Therefore, according to the analysis above in Sections 3.1 to 3.2, an obvious phenomenon can be observed in the MLH distribution in the NCP region: the MLH was lower in southern Hebei than on the northern NCP in spring, autumn and winter but was almost equal to the northern areas in summer.

4. Discussion

4.1 Reasons for low MLH in southern Hebei

Turbulent energy was mainly responsible for the MLH development, and the generation of turbulent energy was highly correlated with the buoyancy flux (mainly heat and moisture fluxes) produced by net radiation and the momentum flux caused by wind shear (*Stull*, 1988). We first compared the net radiation among the BJ, SJZ and TJ observation sites. As shown in Fig. 6, the seasonal net radiation variations were almost consistent among the three stations, and they were high in spring and summer and low in autumn and winter, with annual averages of 5.4, 6.0 and 4.8 W m^{-2}, respectively. The comparable net radiation values at the BJ and SJZ stations indicated that the buoyancy flux was unable to explain the MLH differences between the northern NCP and southern Hebei.

Atmos. Chem. Phys. Discuss., doi:10.5194/acp-2017-295, 2017
Manuscript under review for journal Atmos. Chem. Phys.
Discussion started: 29 May 2017

Atmospheric Chemistry and Physics
Open Access
Discussions

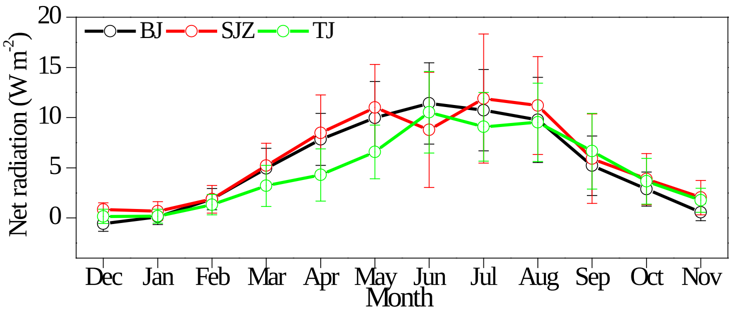

Fig. 6 Monthly variations in net radiation at the BJ, SJZ and TJ sites.

Wind shear was defined and calculated according to Eq. (1):

$$\text{wind shear} = \sqrt{\left(\frac{du}{dz}\right)^2 + \left(\frac{dv}{dz}\right)^2} \qquad (1)$$

where dz is the height difference between two layers at which the vertical wind shear is estimated and du and dv are the differences in zonal and meridional directions in the two different layers (Hyun et al., 2005). Considering the geographic locations (Fig. 1), the lack of sounding data at the SJZ station was addressed by replacement with sounding data from another southern Hebei station (e.g., the XT station); meanwhile, sounding data from another coastal site (e.g., the LT station) were used instead of from the QHD station. Observations were conducted at 8:00 LT and 20:00 LT each day from December 2013 to November 2014, and the wind shear was averaged every 100 m for each sounding profile.

When we analyzed the seasonal means of wind shears between southern Hebei (XT) and the northern NCP (BJ), some distinct features were observed, as shown in Fig. 7. Considering that the regional MLH at 08:00 LT and 20:00 LT was mostly below 300 m (Fig. 4), wind shears in southern Hebei were lower than those in the northern NCP below 300 m but were nearly consistent at the altitude of 300 m both at 08:00 LT and 20:00 LT during the whole year. However, above 300 m at 08:00 LT, wind shears at XT were significantly different from those at BJ again at the altitude of 300-1700 m and, on average, approximately 2.8, 2.5 and 1.9 times smaller than at the BJ stations in spring, autumn and winter, respectively (Figs. 7a, 7c and 7d). The largest discrepancies reached 3.4, 4.3, and 4.5 m s^{-1} km^{-1} in spring, autumn and winter, respectively, and were at the altitude between 500 and 700 m. In summer, the averaged differences narrowed down to only 1.2-fold above 300 m (Fig. 7b). Compared to wind shears at 20:00 LT above 300 m in spring, autumn and winter, mechanical forces were clearly enhanced in BJ at the height of 300-1700 m during the whole night and the turbulent energy was restored in the residual layer. With the increase of solar radiation in the morning, the MLH developed and broke through the residual layer. At this time, the combination of buoyancy and wind shear forces will contribute to a higher MLH at BJ during daytime. Furthermore, the larger wind shears below 300 m during night time at the BJ station could partly explain the higher nocturnal boundary layer on the northern NCP (Fig. 4).

Atmos. Chem. Phys. Discuss., doi:10.5194/acp-2017-295, 2017
Manuscript under review for journal Atmos. Chem. Phys.
Discussion started: 29 May 2017

Atmospheric Chemistry and Physics
Open Access
EGU
Discussions

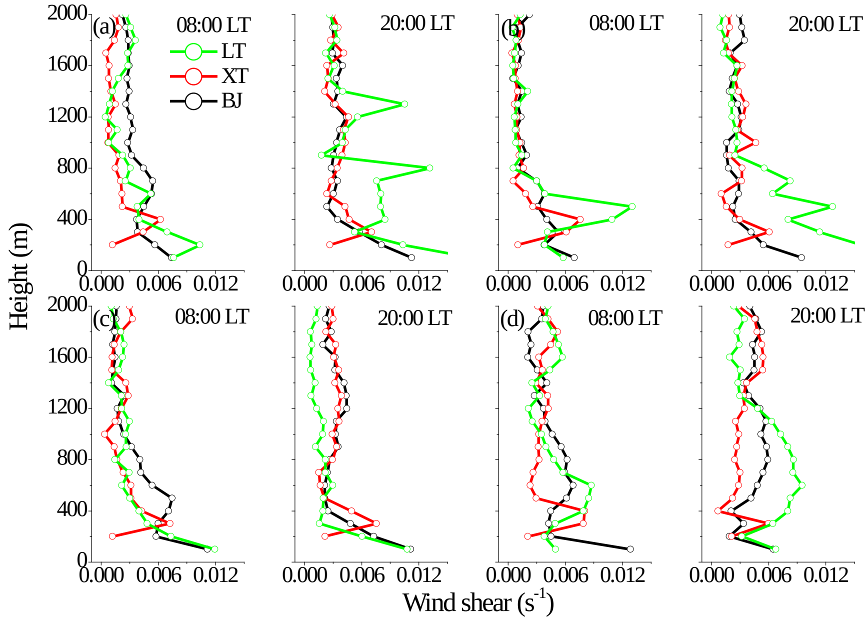

Fig.7 Vertical profiles of wind shear at the BJ, XT and LT stations in (a) spring, (b) summer, (c) autumn and (d) winter.

The lower MLH in southern Hebei was the result of the lessened mechanical forcing due to wind shear at night than occurred in the northern areas in spring, autumn and winter. This pattern could be attributed to the influence of the active fronts passing by under the impact of the Siberian High, and usually, this front system does not reach southern Hebei. In summer, due to the influence of the subtropical high on the NCP and the relatively greater solar radiation, the lessened effects of the front system and strong turbulent exchange will lead to less wind shear contrast in the vertical direction between southern Hebei and the northern NCP.

4.2 Meteorological evidence of serious air pollution in southern Hebei

When we analyzed the near-ground $PM_{2.5}$ and PM_{10} concentrations distribution on the NCP from December 2013 to November 2014, a unique phenomenon was found and shown in Fig. 1 and Fig. S3. The annual means of near-ground $PM_{2.5}$ concentration in southern Hebei (SJZ, XT, HS, HD and DZ) was 124.1μg m^{-3} (218.8 μg m^{-3} for the PM_{10} concentrations), while in the northern areas (BJ, TJ, LF and TS), it was 94.9 μg m^{-3} (145.5 μg m^{-3} for the PM_{10} concentrations), and the difference in near-ground $PM_{2.5}$ concentration between these two areas can be as high as 1.3-fold (1.5-fold for the PM_{10} concentrations). Considering the low MLH in southern Hebei, heavy pollution in southern Hebei may be related with weaker weather conditions, and some other meteorological factors may play a part.

Previous studies revealed that the most significant meteorological factors for regional heavy haze formation on the NCP were RH and MLH (Tang et al., 2016; Zhu et al., 2016). However, due to the lack of wind profiles, Tang et al. (2015) utilized the near-surface WS to estimate the ventilation coefficients (V_c), and the result was not

Atmos. Chem. Phys. Discuss., doi:10.5194/acp-2017-295, 2017
Manuscript under review for journal Atmos. Chem. Phys.
Discussion started: 29 May 2017

sufficiently precise and could not portray the regional pollution dissipation ability accurately. In this study, we utilized wind sounding data to enable an exact evaluation of the regional pollutant dissipation ability. Furthermore, temperature is the main factor in new particle formation, and RH determines the growth rates of particles, which are the most influential meteorological factors for particle formation. As a consequence, in the next section, we will separately analyze the regional particle formation and dissipation ability, each from a meteorological point of view.

4.2.1 Meteorological factors for particle formation

Monthly variations of T and RH are shown in Fig. 8. The T in the southern Hebei was similar to that on the northern NCP in variation pattern and quantity but was approximately 19.3 % higher than at the coastal site (Fig. 8a). Under the same temperature conditions, the new particle formation ability will be the same between these two areas. However, differences existed in RH between southern Hebei and the northern NCP. The RH at the SJZ station was always higher than at the BJ and TJ stations but was slightly lower than at the QHD station through the year (Fig. 8b). The annual averages of RH at the BJ, SJZ, TJ and QHD sites were 51.2, 65.7, 57.0 and 68.6 %, respectively, and the RH at SJZ was 22.1 and 13.2 % higher than at the BJ and TJ sites, respectively (Table S2). As RH is also a key factor for haze development and determines the particle growth rate through hygroscopic growth and secondary formations (Zhao et al., 2013; Fu et al., 2014), even though the new particle formation conditions were the same between these two areas, particles can grow larger under high RH, leading to heavier pollution in southern Hebei.

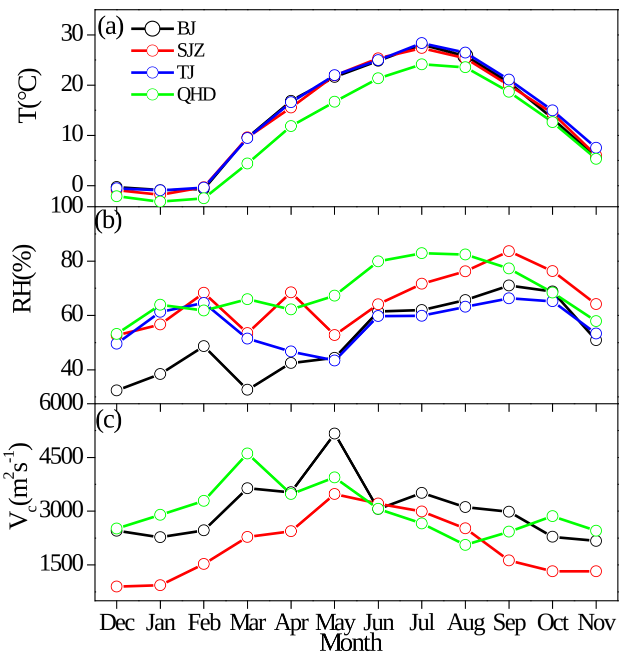

Fig. 8 Seasonal variations of (a) T, (b) RH and (c) V_c at the BJ, SJZ, TJ and QHD stations from December 2013 to November 2014.

4.2.2 Meteorological factors for particle dissipation

As MLH and WS can represent the atmospheric dissipation capability in the vertical and horizontal directions, respectively, in addition to the MLH, we also analyzed the WS variations on the NCP. Similar to our analysis in Section 4.1, as SJZ and QHD had no sounding data and due to the close geographic proximity among SJZ and XT as well as LT and QHD, sounding data from the XT and LT stations were used instead of the data at SJZ and QHD, respectively. The WS profiles were averaged every 100 m at each stations and are depicted in Fig. S2. Except for summer, the WS in southern Hebei was far less than that on the northern NCP and coastal areas both at 08:00 LT and 20:00 LT in spring, autumn and winter (Fig. S2a, S2c and S2d) but was nearly consistent in summer (Fig. S2b). This finding indicated a weaker horizontal diffusion capability in southern Hebei than on the northern NCP and at the coastal sites.

The ventilation coefficient is an important factor in pollutant dissipation and air quality studies; it accounts for the vertical dispersion and advection of pollutants. With larger V_c, strong dissipation ability follows. The V_c is defined as the product of MLH to the wind transport (U_T) and is shown in Eq. (2).

$$V_c = MLH \times U_T \quad (2)$$

When we utilized the wind profiles in Fig. S2 with equal spacing in the vertical direction, U_T could be regarded as the mean wind transport, i.e., $U_T = \frac{1}{n}\sum_{i=1}^{n} U_i$ and U_i is the wind observed at each level and n is the number of levels within the mixing layer (Nair et al., 2007). As the profiles of WS for each station were almost the same in the morning and at night (Fig. S2), it was considered reasonable to regard the sounding data of WS as a climatological constant, and the V_c within the mixing layer could then be calculated. Considering the monthly averaged MLH at the BJ, SJZ and QHD stations, the monthly V_c is depicted in Fig. 8c. V_c at the southern Hebei was always lower than the northern NCP during the whole study period. The seasonal means of V_c at the BJ, SJZ and QHD stations in spring, summer, autumn and winter were 4112.0, 2733.3 and 4008.5; 3227.5, 2908.8 and 2593.7; 2481.4, 1421.9 and 2581.7; and 2397.2, 1117.7 and 2900.0 $m^2\ s^{-1}$, respectively. It was clear that the SJZ station usually had the lowest V_c, and the annual averaged V_c at SJZ was almost 1.5 and 1.5 times smaller than the BJ and QHD stations, respectively (Table S2). As a result, the particle dissipation capability in southern Hebei was much weaker than in the northern and coastal areas.

Therefore, due to the lower atmospheric environment capability, the weaker dissipation ability and stronger particle formation ability, the particles were more easily accumulated and severe haze occurred frequently in southern Hebei. This finding indicated that the industrial structure of southern Hebei is in need of readjustment.

5. Conclusions

To gain new insight into the spatiotemporal variation of the regional MLH, the present study conducted a simultaneous observation with ceilometers at three inland stations (e.g., BJ, SJZ, and TJ) and one coastal site (e.g., QHD) to obtain high spatial and temporal resolution MLH data. The experiment period lasted for 22-months from October 16, 2013, to July 15, 2015, and one year's data (e.g., from December 2013 to November 2014) were utilized for further study. Conclusions were drawn as follows.

The MLH in the inland areas of the NCP was high in spring and summer and low in autumn and winter. Under the effects of sea breeze and a thermal internal boundary layer, the seasonal variation of the MLH in the coastal area of Bohai was different from that of the inland stations, and the lowest MLH was occurred in summer. The MLH peaked earlier at the coastal site in spring and summer than at the inland stations, and this effect weakened with distance from the coast. This effect of sea breeze on coastal MLH was consistent with previous studies, which demonstrated that not only can the mainland MLH be retrieved from ceilometers, but the coastal MLH can be observed with ceilometers.

The MLH in southern Hebei was lower than that on the northern NCP, especially in spring, autumn and winter. As there was little radiation difference between these two areas, the lower MLH in the southern Hebei mainly resulted from the stronger intensity of wind shears on the northern NCP than in southern Hebei at an altitude of 300-1700 m in residual layers. In summer, the wind shear difference lessened, and the MLHs between the southern and northern areas were nearly consistent.

From a meteorological point of view, the weaker atmospheric environment capability combined with the weaker pollutant dissipation ability and the stronger pollutant formation ability will cause severe haze to occur easily in southern Hebei, and the industrial layout in southern Hebei is in need of restructuring. Heavily polluting enterprises should be relocated to locations with better weather conditions (e.g., certain northern areas and coastal areas), and strong emission reduction measures should be implemented in the remaining industrial enterprises to improve air quality.

Overall, the present study is the first to conduct a long-term observation of the MLH with high spatial resolution on a regional scale. The observation results will be of great importance for model parameterization scheme promotion and provide basic information for the distribution of weather conditions in the NCP region. The deficiency of this study is that we took no account of the transport effect on $PM_{2.5}$ concentrations. Because pollutants are usually transported from south to north in the NCP region during haze episodes (Zhu et al., 2016; Tang et al., 2015), the pollutant transport has a greater impact on northern areas and had less of an influence on the results of this analysis. The absence of sounding data at noon is another shortcoming, and we plan to conduct daytime observations in future experiments. Nevertheless, our study can provide reasonable and scientific suggestions for industrial layout and air pollution emissions reduction measures for the NCP region, which will be of great importance for achieving the integrated development goals.

Acknowledgments

This work was supported by the CAS Strategic Priority Research Program (Grant no.XDB05020000), the National Natural Science Foundation of China (Grant no.41230642) and the National Earth System Science Data Sharing Infrastructure, National Science & Technology Infrastructure of China

References

Beyrich, F.: Mixing height estimation from SODAR data – a critical discussion, Atmos. Environ., 31, 3941–3953, 1997.

Chen, W., Kuze, H., Uchiyama, A., Suzuki, Y., and Takeuchi, N.: One-year observation of urban mixed layer characteristics at Tsukuba, Japan using a micro pulse lidar, Atmos. Environ., 35, 4273–4280, doi:10.1016/S1352-2310(01)00181-9, 2001.

Emeis, S., C. Münkel, S. Vogt, W. J. Müller, and K. Schäfer: Atmospheric boundary-layer structure from simultaneous SODAR, RASS, and ceilometer measurements, Atmos. Environ., 38(2), 273-286, doi:10.1016/j.atmosenv.2003.09.054, 2004.

Emeis, S., K. Schäfer, and C. Münkel: Observation of the structure of the urban boundary layer with different ceilometers and validation by RASS data, Meteorologische Zeitschrift, 18(2), 149-154, doi:10.1127/0941-2948/2009/0365, 2009.

Emeis, S., K. Schäfer, C. Münkel, R. Friedl, and P. Suppan: Evaluation of the Interpretation of Ceilometer Data with RASS and Radiosonde Data, Bound.-Lay. Meteorol., 143(1), 25-35, doi:10.1007/s10546-011-9604-6, 2011.

Eresmaa, N., Karppinen, A., Joffre, S. M., Räsänen, J., and Talvitie, H.: Mixing height determination by ceilometer, Atmos. Chem. Phys., 6, 1485–1493, doi: 10.5194/acp-6-1485-2006, 2006.

Fu, G., W. Xu, R. Yang, J. Li, and C. Zhao: The distribution and trends of fog and haze in the North China Plain over the past 30 years, Atmos. Chem. Phys., 14 (21), 11949-11958, 2014.

Guo, J.,Y. Miao, Y. Zhang, H. Liu, Z. Li, W. Zhang, J. He, M. Lou, Y. Yan, L. Bian, and P. Zhai: The climatology of planetary boundary layer height in China derived from radiosonde and reanalysis data, Atmos. Chem. Phys., 16(20), 13309-13319, doi:10.5194/acp-16-13309-2016, 2016.

Guo, J.P., X.Y. Zhang, Y.R. Wu, H.Z. Che, Laba, and X. Li: Spatio-temporal variation trends of satellite-based aerosol optical depth in China during 1980-2008, Atmos. Environ., 45(37), 6802-6811,doi: 10.1016/j.atmosenv.2011.03.068,2011.

He, Q. and Mao, J.: Observation of urban mixed layer at Beijing using a micro pulse lidar, Acta Meteorol. Sin., 63, 374–384, 2005.

Hu, X., Ma, Z., Lin, W., Zhang, H., Hu, J., Wang, Y., Xu, X., Fuentes, J. D. and Xue, M.: Impact of the Loess Plateau on the atmospheric boundary layer structure and air quality in the North China Plain?: A case study, Sci. Total Environ., 499, 228–237, doi:10.1016/j.scitotenv.2014.08.053, 2014.

Hu, B., Wang, Y. S., and Liu, G. R.: Relationship between net radiation and broadband solar radiation in the Tibetan Plateau, Adv. Atmos. Sci., 29, 135-143, doi: 10.1007/s00376-011-0221-6, 2012.

Huang, Q.-Q., X.-H. Cai, Y. Song, and L. Kang: A Numerical Study of Sea Breeze

Atmos. Chem. Phys. Discuss., doi:10.5194/acp-2017-295, 2017
Manuscript under review for journal Atmos. Chem. Phys.
Discussion started: 29 May 2017

and Spatiotemporal Variation in the Coastal Atmospheric Boundary Layer at Hainan Island, China, Bound.-Lay. Meteorol., 161(3), 543-560, doi:10.1007/s10546-016-0177-2, 2016.

Ji, D., Y. Wang, L. Wang, L. Chen, B. Hu, G. Tang, J. Xin, T. Song, T. Wen, Y. Sun, Y. Pan, Z. Liu: Analysis of heavy pollution episodes in selected cities of northern China, Atmos. Environ., 50(2012), 338-348, 2012.

Li M., G. Tang, J. Huang, Z. Liu, J. An, and Y. Wang: Relationship between atmospheric MLH and winter haze pollution in the Jing-Jin-Ji region, Environ. Sci., 2015,(06):1935-1943, 2015.

Li, P., J. Xin, X. Bai, Y. Wang, S. Wang, S. Liu, and X. Feng: Observational studies and a statistical early warning of surface ozone pollution in Tangshan, the largest heavy industry city of North China, Inter. J. Env. Res. Pub. Heal., 10(3), 1048-1061, doi:10.3390/ijerph10031048, 2013.

Liu, Z., B. Hu, J. Zhang, Y. Yu, and Y. Wang: Characteristics of aerosol size distributions and chemical compositions during wintertime pollution episodes in Beijing, Atmos. Res., 168, 1-12, doi:10.1016/j.atmosres.2015.08.013, 2016.

Miao, Y., X.-M. Hu, S. Liu, T. Qian, M. Xue, Y. Zheng, and S. Wang: Seasonal variation of local atmospheric circulations and boundary layer structure in the Beijing-Tianjin-Hebei region and implications for air quality, J. Adv. Model. Earth. Sy. , 7(4), 1602-1626, doi:10.1002/2015ms000522, 2015.

Münkel, C., and J. Räsänen: New optical concept for commercial lidar ceilometers scanning the boundary layer, P.SPIE, 5571, 364-374, 2004.

Münkel, C., N. Eresmaa, J. Räsänen, and A. Karppinen: Retrieval of mixing height and dust concentration with lidar ceilometer, Bound.-Lay. Meteorol., 124(1), 117-128, doi:10.1007/s10546-006-9103-3, 2006.

Muñoz, R. C., and A. A. Undurraga: Daytime Mixing layer over the Santiago Basin: Description of Two Years of Observations with a Lidar Ceilometer, J. Appl. Meteorol. Clim., 49(8), 1728-1741, doi:10.1175/2010jamc2347.1, 2010.

Puygrenier, V., F. Lohou, B. Campistron, F. Saïd, G. Pigeon, B. Bénech, and D. Serça: Investigation on the fine structure of sea-breeze during ESCOMPTE experiment, Atmos. Res., 74(1–4), 329-353, doi:http://dx.doi.org/10.1016/j.atmosres.2004.06.011, 2005.

Quan, J., Gao, Y., Zhang, Q., Tie, X., Cao, J., Han, S., Meng, J., Chen, P., and Zhao, D.: Evolution of planetary boundary layer under different weather conditions, and its impact on aerosol concentrations, Particuology, 11, 34–40, doi:10.1016/j.partic.2012.04.005, 2013.

Schween, J. H., A. Hirsikko, U. Löhnert, and S. Crewell: Mixing-layer height retrieval with ceilometer and Doppler lidar: from case studies to long-term assessment, Atmos. Meas. Tech., 7(11), 3685-3704, doi:10.5194/amt-7-3685-2014, 2014.

Seibert, P., F. Beyrich, S.-E. Gryning, S. Joffre, A. Rasmussen, and P. Tercier: Review and intercomparison of operational methods for the determination of the mixing height, Atmos. Environ., 34(7), 1001-1027, doi:http://dx.doi.org/10.1016/S1352-2310(99)00349-0, 2000.

Seidel, D. J., C. O. Ao, and K. Li: Estimating climatological planetary boundary layer heights from radiosonde observations: Comparison of methods and uncertainty analysis, J. Geophys. Res., 115, D16113, doi:10.1029/2009JD013680, 2010.

Sokół, P., I. Stachlewska, I. Ungureanu, and S. Stefan: Evaluation of the boundary layer morning transition using the CL-31 ceilometer signals, Acta Geophys., 62(2), doi:10.2478/s11600-013-0158-5, 2014.

Stull, R.B.: An Introduction to Boundary Layer Meteorology, Kluwer Academic Publishers, Dordrecht, 1988.

Tang, G., J. Zhang, X. Zhu, T. Song, C. Münkel, B. Hu, K. Schäfer, Z. Liu, J. Zhang, L. Wang, J. Xin, P. Suppan, and Y. Wang: Mixing layer height and its implications for air pollution over Beijing, China, Atmos. Chem. Phys., 16(4), 2459-2475, doi:10.5194/acp-16-2459-2016, 2016.

Tang, G., P. Zhao, Y. Wang, W. Gao, M. Cheng, J. Xin, X. Li, Y. Wang: Mortality and air pollution in Beijing: the long-term relationship. Atmos. Environ., 150, 238-243, doi: 10.1016/j.atmosenv.2016.11.045, 2017a.

Tang, G., X. Li, Y. Wang, J. Xin, and X. Ren: Surface ozone trend details and interpretations in Beijing, 2001–2006, Atmos. Chem. Phys., 9, 8813-8823, doi:10.5194/acp-9-8813-2009, 2009.

Tang, G., X. Zhu, B. Hu, J. Xin, L. Wang, C. Münkel, G. Mao, and Y. Wang: Impact of emission controls on air quality in Beijing during APEC 2014: lidar ceilometer observations, Atmos. Chem. Phys., 15(21), 12667-12680, doi:10.5194/acp-15-12667-2015, 2015.

Tang, G., X. Zhu, J. Xin, B. Hu, T. Song, Y. Sun, J. Zhang, L. Wang, M. Cheng, N. Chao, L. Kong, X. Li, Y Wang. Modelling study of boundary-layer ozone over northern China - Part I: Ozone budget in summer. Atmos. Res., 187, 128-137, 2017b.

Tang, G., Y. Wang, X. Li, D. Ji, S. Hsu, and X. Gao: Spatial-temporal variations in surface ozone in Northern China as observed during 2009–2010 and possible implications for future air quality control strategies, Atmos. Chem. Phys., 12, 2757-2776, doi:10.5194/acp-12-2757-2012, 2012.

Tomasi, F. D., M. M. Miglietta, M. R. Perrone: The Growth of the Planetary Boundary Layer at a Coastal Site: a Case Study, Bound.-Lay. Meteorol., 139:521-541, doi: 10.1007/s10546-011-9592-6, 2011.

Tu J., S. Zhang, X. Cheng, W. Yang, Y. Yang: Temporal and Spatial Variation of Atmospheric Boundary Layer Height(ABLH) over the Yellow East China Sea, J. Ocean U. China, 42(4):7-18, 2012.

van der Kamp, D., and I. McKendry: Diurnal and Seasonal Trends in Convective Mixed-Layer Heights Estimated from Two Years of Continuous Ceilometer Observations in Vancouver, BC, Bound.-Lay. Meteorol., 137(3), 459-475, doi:10.1007/s10546-010-9535-7, 2010.

Vijayakumar S. Nair, K. K. Moorthy, D. P. Alappattu, P. K. Kunhikrishnan, S. George, P. R. Nair, S. S. Babu, B. Abish, S. K. Satheesh, S. N. Tripathi, K. Niranjan, B. L. Madhavan, V. Srikant, C. B. S. Dutt, K. V. S. Badarinath, and R. R. Reddy: Wintertime aerosol characteristics over the Indo-Gangetic Plain (IGP): Impacts of local boundary layer processes and long-rang transport, J. Geo. Res.:

2006JD008099, doi:10.1029/2006JD008099, 2007.

Wagner, P., K. Schäfer: Influence of mixing layer height on air pollutant concentrations in an urban street canyon, Urban Climate, http://dx.doi.org/10.1016/j.uclim.2015.11.001, 2015.

Wang, L., N. Zhang, Z. Liu, Y. Sun, D. Ji, and Y. Wang: The Influence of Climate Factors, Meteorological Conditions, and Boundary-Layer Structure on Severe Haze Pollution in the Beijing-Tianjin-Hebei Region during January 2013, Adv. Meteorol., 2014, 1-14, doi:10.1155/2014/685971, 2014.

Wang, Y., L. Yao, L. Wang, Z. Liu, D. Ji, G. Tang, J. Zhang, Y. Sun, B. Hu, and J. Xin: Mechanism for the formation of the January 2013 heavy haze pollution episode over central and eastern China, Sci. China Earth Sci., 57(1), 14-25, doi:10.1007/s11430-013-4773-4, 2013.

Wiegnerm, M., F. Madonna, I. Binietoglou, R. Forkel, J. Gasteiger, A. Geiβ, G. Pappalardo, K. Schäfer, and W. Thomas: What is the benefit of ceilometers for aerosol remote sensing? An answer from ERALINET, Atmos. Meas. Tech., 7, 1979-1997, doi: 10.5194/amt-7-1979-2014, 2014.

Xin, J., Y. Wang, Y. Pan, D. Ji, Z. Liu, T. Wen, Y. Wang, X. Li, Y. Sun, J. Sun, P. Wang, C. Wang, X. Wang, Z. Cong, T. Song, B. Hu, L. Wang, G. Tang, W. Gao, Y. Guo, H. Miao, S. Tian, and L. Wang: The Campaign on Atmospheric Aerosol Research Network of China: CARE-China, Bull. Amer. Meteor. Soc., 96(7), 1137-1155, doi:10.1175/bams-d-14-00039.1, 2015.

Xu, R., G. Tang, Y. Wang, and X. Tie: Analysis of a long-term measurement of air pollutants (2007-2011) in North China Plain (NCP); Impact of emission reduction during the Beijing Olympic Games, Chemosphere, 159, 647-658, doi:10.1016/j.chemosphere.2016.06.025, 2016.

Yu-Kyung, H., K.-E. Kim, and K.-J. Ha: A comparison of methods to estimate the height of stable boundary layer over a temperate grassland, Agr. Forest Meteorol.: 132(2005) 132-142, 2005.

Zhang Z., X. Cai, Y. Song, L. Kang, X. Huang, Q. Li: Temporal and spatial variation of atmospheric boundary layer height over Hainan Island and its adjacent sea areas, Acta. Sci. Nat. Univ. Pekin., 49:83-90, doi: 10.13209/j.0479-8023.2013.105, 2013.

Zhang, H., Y. Wang, J. Hu, Q. Ying, and X.-M. Hu: Relationships between meteorological parameters and criteria air pollutants in three megacities in China, Environ. Res., 140, 242–254, doi:10.1016/j.envres.2015.04.004, 2015.

Zhang, J. K., Y. Sun, Z. R. Liu, D. S. Ji, B. Hu, Q. Liu, and Y. S. Wang: Characterization of submicron aerosols during a month of serious pollution in Beijing, 2013, Atmos. Chem. Phys., 14(6), 2887-2903, doi:10.5194/acp-14-2887-2014, 2014.

Zhang, W., J. Guo, Y. Miao, H. Liu, Y. Zhang, Z. Li, and P. Zhai: Planetary boundary layer height from CALIOP compared to radiosonde over China, Atmos. Chem. Phys., 16, 9951–9963, doi: 10.5194/acp-16-9951-2016, 2016.

Zhao, X., P. Zhao, J. Xu, W. Meng, W. Pu, F. Dong, D. He, and Q. Shi: Analysis of a winter regional haze event and its formation mechanism in the North China Plain, Atmos. Chem. Phys., 13 (11), 5685-5696, 2013.

Zhu, X., G. Tang, B. Hu, L. Wang, J. Xin, J. Zhang, Z. Liu, C. Münkel, and Y. Wang: Regional pollution and its formation mechanism over North China Plain: A case study with ceilometer observations and model simulations, J. Geo. Res.: Atmos., 2016JD025730, doi:10.1002/2016JD025730, 2016.